Supporting Information

Crawford et al. 10.1073/pnas.0902366106

SI Text

SI Methods. ***Metabolite and insulin analyses.*** Fed and 24-hour-fasting levels of glucose and free fatty acids were measured in sera (or from evaporated chloroform-methanol extracts of liver) by using standard biochemical methods (Wako), as were triglyceride concentrations (Infinity Triglycerides) and insulin (Millipore). Myocardial glycogen assays were performed as described in ref. 3. Briefly, 10 mg of a freeze-clamped ventricle from each mouse was homogenized in 400 μL of ice-cold 0.2 M NaOH/1 mM EDTA, and an 80 μL aliquot was heated 95 °C for 5 min. For protein concentration and normalization, a 2 μL aliquot was added to 0.8 mL water plus 0.2 mL Bradford dye (Bio-Rad), incubated for 10 min at room temperature, and absorbance read at 595 nm. Five microliters of this fresh alkali extract (≈25 μg protein) were added to 0.5 mL of glycogen reagent [50 mM sodium acetate, pH 4.6, 0.02% BSA, with and without 5 μg/mL *Aspergillus niger* amyloglucosidase (Roche, 14 units/mg)]. The mixture was subsequently incubated for 30 min at 25 °C. One-half milliliter of glucose reagent [100 mM Tris·HCl, pH 8.1, 2 mM MgCl2, 1 mM DTT, 1 mM ATP, 0.2 mM $NADP^+$, 5 μg/mL *Leuconostoc mesenteroides* glucose 6-phosphate dehydrogenase (Calbiochem, 220 units/mg), and 20 μg/mL *Saccharomyces cerevisiae* hexokinase (Sigma, 250 units/mg)] was added and the mixture incubated for 30 min at 25 °C. The NADPH generated from $NADP^+$ was measured fluorometrically (excitation, 360 nm; emission, 460 nm).

Transmission EM studies of myocardial mitochondrial morphology. Ventricles were dissected from CO_2-euthanized animals, rapidly diced into 2–3-mm^3 pieces, washed in PBS, and fixed overnight at 4 °C in a solution containing 2% paraformaldehyde, 2.5% glutaraldehyde, and 1% tannic acid (prepared in 0.1 M cacodylic acid, pH 7.2). After multiple rinses in 0.1 M cacodylic acid, samples were fixed in 1% osmium tetroxide/0.1 M cacodylic acid for 1 h, stained for 1 h in 1% uranyl acetate (prepared in distilled, deionized water), dehydrated through a series of graded ethanols and propylene oxide, and then infiltrated with and embedded in monomeric Embed 812 (Electron Microscopy Sciences). Seventy-five-nanometer-thick sections were cut from each block, placed on grids, stained with Reynolds' lead citrate/1% uranyl acetate, and viewed under a Hitachi H7500 transmission electron microscope.

Mitochondrial qPCR. Hearts were dissected from CO_2-euthanized animals and snap-frozen in liquid N_2. Ventricular samples (≈10 mg) were cut on dry ice by using a razor blade. Each sample was placed in 75 μL of lysis solution (25 mM NaOH, 0.2 mM EDTA, pH 12), incubated at 94 °C for 20 min, and then cooled to 4 °C for 5 min. Seventy-five microliters of neutralization solution (40 mM Tris·HCl, pH 5) was subsequently added, and a 1-μL aliquot of this mixture was used as template for qPCR. The ratio of mitochondrial DNA (mtDNA) to nuclear DNA (nDNA) was determined by using primers against mt*Cytb* (mtDNA) and *Rpl32* (nDNA) (Table S6). The mtDNA/nDNA ratio was arbitrarily set at 1 for fed GF hearts.

In vitro assays of mitochondrial respiration. Myocardial mitochondria were isolated from CO_2-euthanized mice by sucrose gradient centrifugation (1). Briefly, ventricles were excised, rinsed in ice-cold Mitochondrial Isolation Medium (MIM, 10 mM Na Hepes, pH 7.2, 300 mM sucrose, 0.2 mM EDTA), and minced with fine scissors in a dry Petri dish (maintained on ice). The minced tissue from each heart was incubated for 15 min at 4 °C in 5 mL of bovine pancreatic trypsin (Sigma; specific activity ≥9,000 Na-Benzoyl-L-Arginine Ethly Ester (BAEE) units/mg protein; 125 μg/mL MIM). Five milliliters of ice-cold MIM (pH 7.4) containing BSA (Sigma; 1 mg/mL) and soybean trypsin inhibitor (Sigma; 650 μg/mL) was subsequently added to the preparation. Tissue fragments were then allowed to settle by gravity, the supernatant was removed, and fresh ice-cold MIM-BSA (pH 7.4) was added. The samples were subsequently homogenized on ice by using a Glas-Col dounce homogenizer, and centrifuged at 600 × *g* for 10 min at 4 °C. The resulting supernatant, which contained mitochondria, was spun at 8,000 × *g* for 15 min at 4 °C, the supernatant discarded, the mitochondrial pellet resuspended in 10 mL of ice-cold MIM-BSA, and the sample centrifuged again at 8,000 × *g* for 15 min at 4 °C. The pellet was briefly washed in ice-cold MIM, and resuspended in 75 μL of ice-cold MIM (pH 7.2) per heart. Mitochondrial preparations were maintained on ice and used for respiration assays on the same day as the isolation. Protein content was quantified by Bradford assay (Bio-Rad); 0.5 mg of mitochondrial protein was used for each respiration assay.

Respiration assays were performed at 37 °C by using a water-jacketed Clark electrode (Hansatech Instruments) and conditions described previously (2). Briefly, 1 mL of respiration buffer (20 mM Hepes, pH 7.1, 125 mM KCl, 3 mM magnesium acetate, 5 mM KH_2PO_4, 0.4 mM EGTA, 0.3 mM DTT, 2 mg BSA per mL) was used to supply one of 2 substrate combinations: (*i*) 20 μM palmitoyl-L-carnitine plus 5 mM malate; or (*ii*) 10 mM pyruvate plus 5 mM malate. The solubility of oxygen in the respiration buffer at 37 °C was 235 nmol O_2 per mL. Following measurement of basal (state 2) respiration, 1 mM ADP was added to isolated mitochondria in respiration buffer, and maximal (state 3) respiration defined. Thereafter, state 4 (ADP-depleted) respiration was mimicked by adding 1 μg/mL oligomycin (Sigma) to inhibit ATP synthase.

Western blots. Snap-frozen specimens consisting of both ventricles from a given animal were homogenized (Teflon pestle) in 2 mL of ice-cold tissue extraction buffer [20 mM Tris, pH 7.5; 150 mM NaCl, 1 mM EDTA, 1% Triton X-100, plus protease inhibitor mixture (Roche) and phosphatase inhibitors (Sigma)]. Cellular debris were removed by centrifugation (12,000 × *g* at 4 °C for 15 min) and the protein concentration of the resulting supernatant was determined (bicinchoninic acid assay; Pierce). Twenty micrograms of protein were loaded per lane of SDS/PAGE gel and transferred to PVDF membranes (Invitrogen). Membranes were treated with blocking buffer [5% nonfat dry milk in Tris-buffered saline plus 0.1% Tween-20 (TBST)], washed in TBST, and then incubated overnight at 4 °C with rabbit polyclonal antibodies against phospho-Akt1 (Ser-473), phospho-AMPKα (Thr-172), total Akt, total AMPKα (Cell Signaling Technologies) or actin (Sigma) in a solution of 5% BSA/TBST (all primary antibodies were diluted 1:1,000). After washing in TBST, membranes were incubated in donkey anti-rabbit sera conjugated to horseradish peroxidase (diluted 1:5,000 in TBST; GE Healthcare), washed again in TBST, and incubated in ECL Plus reagents (GE Healthcare). Following exposure of film, band intensity was quantified (QuantityOne software package;Bio-Rad).

Echocardiography. Transthoracic echocardiography was performed under light anesthesia (Avertin; 0.05 mg/g body weight, administered i.p.). An Acuson Sequoia 256 Echocardiography System equipped with a 13-MHz linear array ultrasound transducer was used to acquire images. The parasternal long-axis image was used to measure maximum left ventricle (LV) length. Five to seven consecutive 2D short-axis images of the LV were

obtained at several levels along the longitudinal axis (from the base to the apex of the heart) by using established anatomical landmarks. Endocardial and epicardial borders were traced by using electronic calipers. LV volumes were calculated by adding the volumes of each short-axis cross-sectional slab. In addition to the standard parameters determined by 2D-guided M-mode, Doppler indices of diastolic function were obtained, including transmitral flow velocities of E waves (i.e., the velocity of blood flow between the left atrium and ventricle in early diastole), plus tissue Doppler imaging (TDI) of mitral valve apparatus displacement [E′ (4)]. Assessment of Doppler waveforms required administration of a sinus node inhibitor (Zatebradine, 0.01 mg/g i.p.).

Exercise training of gnotobiotic mice in gnotatoria. A swimming protocol was developed for gnotobiotic mice that allowed them to remain in their isolators for the duration of the training period. The isolators contained autoclaved plastic mouse-cage bottoms that were used as swimming tanks. During training sessions, a circulating water-heating pad was placed under the swimming tanks on the outside of the flexible film (Trexler-style) gnotobiotic isolator. On a twice-daily basis, tap water was autoclaved in glass bottles, which were then closed tightly and transported, while still warm, through the gnotobiotic isolator port, in a mist of sterilizing aerosolized chlorine dioxide (Clidox-S, Pharmacal Research Technologies, Inc.). Once the autoclaved water was poured into the swimming tanks and the temperature confirmed to be 32–35 °C, 2–3 gnotobiotic mice were placed into each tank [a total of 5 germ-free (GF) and 5 ''conventionalized'' (CONV-D) mice were subjected to this exercise regimen, in separate gnotobiotic isolators].

On the first day of the protocol, animals swam in two 10-min sessions separated by a 3-h interval. On subsequent days, the duration of each swimming session was increased in 10-min increments, until 90-min sessions were achieved twice per day. Thereafter, this level of exercise was sustained for a total of 30 days, 5 days per week (weekdays only). During the incremental phase of the protocol, the swimming duration was maintained at the Friday level on the following Monday before increasing again. Echocardiograms were performed on the day the mice were killed, which occurred on the morning immediately after the thirtieth day of exercise.

Determination of lean mass. Unanesthetized mice were gently placed into a plastic cylinder tube that was then inserted into an Echo MRI (Echo Medical Systems) for determination of total, lean, and adipose mass. Routine measurements required no more than 1 min of data collection per animal.

16S rRNA-based enumeration studies of the gut microbiota. Four groups of CONV-D mice were studied: controls consuming the CARB diet, fasted animals who had been subjected to 24 h of withdrawal from the CARB diet, mice that had consumed the high-fat, low-carbohydrate ketogenic diet for 30 days, and mice that had been trained by swimming in the gnotatorium for 30 days while consuming the standard low-fat, polysaccharide-rich chow CARB diet (n = 4–5 animals per group, per experiment).

Cecal contents were harvested from each animal at the time of death and rapidly frozen in liquid N_2. Samples (100 mg) were suspended in 500 μL of buffer A (200 mM Tris, pH 8.0, 200 mM NaCl, 20 mM EDTA), followed by addition of 210 μL of 20% SDS, and 500 μL of a 1:1 mixture of phenol/chloroform. Five-hundred microliters of zirconium beads were added to each tube, which were then placed in a bead beater (Biospec; highest setting for 2 min). The mixture was then spun at 6,000 × g at 4 °C for 3 min and DNA was purified from the resulting supernatant by phenol/chloroform extraction followed by ethanol precipitation.

The cecal microbiota of CONV-D mice were compared by using multiplex pyrosequencing of error-correcting, barcoded amplicons, generated from the V2 region their bacterial 16S rRNA genes (5). A total of 145,428 reads that passed quality control (6) were generated from the 38 samples that yielded sufficient PCR products (range = 984–24,156 reads per sample).

The degree of similarity of the different gut communities was measured by using the UniFrac metric. Sequence reads were grouped into operational taxonomic units (OTUs) based on a threshold cutoff of ≥97% identity (7). A phylogenetic tree was built from one representative sequence from each OTU by using Clearcut's relaxed neighbor joining implementation with the Kimura 2-parameter correction for distances (8) and the tree used for unweighted and weighted UniFrac analysis (the latter takes into account abundance of phylotypes). A matrix of UniFrac distance measurements for all pairwise comparisons of communities was constructed and used to generate Principal Coordinates Analysis (PCoA) plots (9). Samples were analyzed in 2 ways: By using all reads or a maximum of 1,000 randomly selected reads.

SI Results: Functional Genomic Studies of Myocardial Physiological Hypertrophy. GeneChip datasets disclosed that the significantly increased myocardial mass observed in CARB-fed CONV-D compared with GF animals is not associated with significant changes in expression of biomarkers of ''pathological'' cardiac hypertrophy, such as Acta1 (α-skeletal muscle actin), Myh7 (β-myosin heavy chain), Nppa and Nppb (atrial and brain natriuretic peptides, respectively), Ednra and Ednrb (endothelin receptor types A and B, respectively), Ucp2 (uncoupling protein 2), Ace (angiotensin converting enzyme), and Adrbk1/GRK2 (β-adrenergic receptor kinase 1) (10). Therefore, we determined whether the functional genomic differences between CARB-fed GF and CONV-D mice were differences that are also seen in the context of ''physiological hypertrophy''.

To address this question, we began with the GeneChip dataset comparison shown in Fig. S7*A*, which yielded a list of 170 genes that were significantly up- or down-regulated in the heart after conventionalization (Fig. S7*B* and Table S5). This comparison was organized as follows: (*i*) dChip was first used to generate a list of genes that were up- or down-regulated ≥1.5-fold in the hearts of wild-type versus *Pparα*−/− GF or CONV-D mice; (*ii*) the resulting set of genes was then queried for those that exhibited a statistically significant 1.2-fold difference between wild-type GF and CONV-D hearts. All genes that emerged from these comparisons met the following criteria: Their fold-differences in expression between the experimental and control groups had a lower-bound 90% confidence interval; the P value (Student's t test) for the observed fold-difference in expression was <0.05; the gene was called present in 100% of the RNA samples where higher relative expression was observed; the minimal intensity after normalization of signals across the GeneChips was >100 (note that the normalized mean signal intensity was set at 500); and the false discovery rate was <1%.

Ingenuity Pathways Analysis (IPA) of the resulting list of 64 genes whose expression was significantly higher in the hearts of CARB-fed CONV-D versus GF mice indicated that they were significantly enriched in functions (pathways) related to fatty acid and lipid metabolism, β-alanine metabolism, propanoate metabolism, branch-chain amino acid metabolism, and antigen presentation. On the other hand, the list of 106 genes whose expression was significantly higher in the hearts of GF animals were enriched in functions related to actin cytoskeleton signaling, extracellular matrix–receptor interaction, cell adhesion, integrin signaling, vascular development, and leukocyte extravasation.

To determine whether these differences share features with changes that occur with the physiological hypertrophy that normally takes place when conventionally raised mice are exercised, we turned to GeneChip datasets deposited by the Cardiogenomics consortium from their studies of the hearts of

untrained conventionally raised (CONV-R) FVB/N female mice that swam for just 10 min (control) versus those subjected to a 4-week-long swimming regimen (http://cardiogenomics.med-.harvard.edu/groups/proj1/pages/download swim.html).

When we evaluated the Cardiogenomics dataset by using IPA, we found that the group of 114 significantly up-regulated genes in trained versus untrained CONV-R mice was enriched in a number of the pathways that were also enriched in the 64 up-regulated genes culled from our comparison of the hearts of untrained CARB-fed CONV-D versus GF mice. These pathways included fatty acid metabolism, branch-chain amino acid degradation, and propanoate metabolism. The same was true of the 106 down-regulated genes culled from our comparison of untrained CONV-D versus GF animals. Enriched pathways that were common to this comparison and the comparison of trained versus untrained CONV-R mice included actin cytoskeleton, integrin signaling, and leukocyte extravasation. Taken together, these findings led us to conclude that the increase in myocardial mass that occurs when GF mice are colonized is accompanied by transcriptional responses that are similar to those encountered during physiological hypertrophy.

1. Boehm EA, et al. (2001) Increased uncoupling proteins and decreased efficiency in palmitate-perfused hyperthyroid rat heart. *Am J Physiol* 280:H977–H983.
2. Lehman JJ, et al. (2008) The transcriptional coactivator PGC-1alpha is essential for maximal and efficient cardiac mitochondrial fatty acid oxidation and lipid homeostasis. *Am J Physiol* 295:H185–H196.
3. Lin SS, Manchester JK, Gordon JI (2001) Enhanced gluconeogenesis and increased energy storage as hallmarks of aging in *Saccharomyces cerevisiae*. *J Biol Chem* 276:36000–36007.
4. Chiu HC, et al. (2005) Transgenic expression of fatty acid transport protein 1 in the heart causes lipotoxic cardiomyopathy. *Circ Res* 96:225–233.
5. Hamady M, et al. (2008) Error-correcting barcoded primers for pyrosequencing hundreds of samples in multiplex. *Nat Methods* 5:235–237.
6. Fierer N, et al. (2008) Short-term temporal variability in airborne bacterial and fungal populations. *Appl Environ Microbiol* 74:200–207.
7. Ley RE, et al. (2008) Evolution of mammals and their gut microbes. *Science* 320:1647–1651.
8. Sheneman L, Evans J, Foster JA (2006) Clearcut: A fast implementation of relaxed neighbor joining. *Bioinformatics* 22:2823–2824.
9. Lozupone C, Knight R (2005) UniFrac: A new phylogenetic method for comparing microbial communities. *Appl Environ Microbiol* 71:8228–8235.
10. Dorn GW, II (2007) The fuzzy logic of physiological cardiac hypertrophy. *Hypertension* 49:962–970.

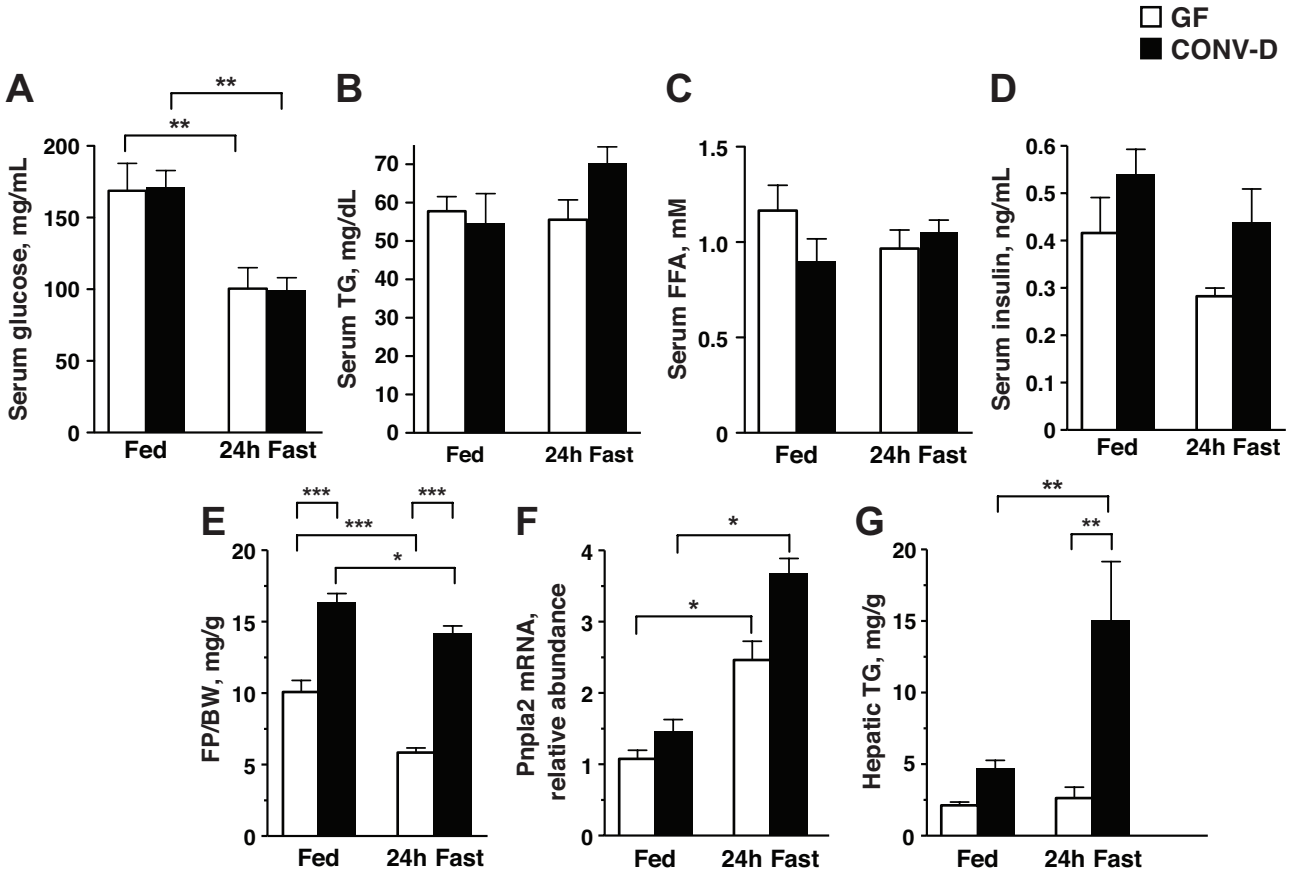

Fig. S1. Key metabolites and effectors of insulin signaling and lipid mobilization in fed and fasted GF and CONV-D wild-type C57BL/6J mice. Mice were fed the standard CARB diet. (*A–D*) Serum glucose (*A*), triglycerides (TG) (*B*), and free fatty acids (FFA) (*C*) and insulin (*D*) were measured (mean values ± SEM; n = 10 animals per treatment group). (*E*) Epididymal fat pad (FP) to body weight (BW) ratio. Both fat pads were measured per animal and the values combined to calculate the FP/BW (n = 10 mice per treatment group). (*F*) qRT-PCR assays of Pnpla2 mRNA levels in epididymal fat pads; data were normalized to the levels of Rp132 by using the $\Delta\Delta C_T$ method (n = 5 animals per treatment group). (*G*) Hepatic triglyceride levels (expressed as mg per weight of liver; n = 5 mice per group). *, $P < 0.05$; **, $P < 0.01$; ***, $P < 0.001$ (2-way ANOVA with posthoc Bonferroni test).

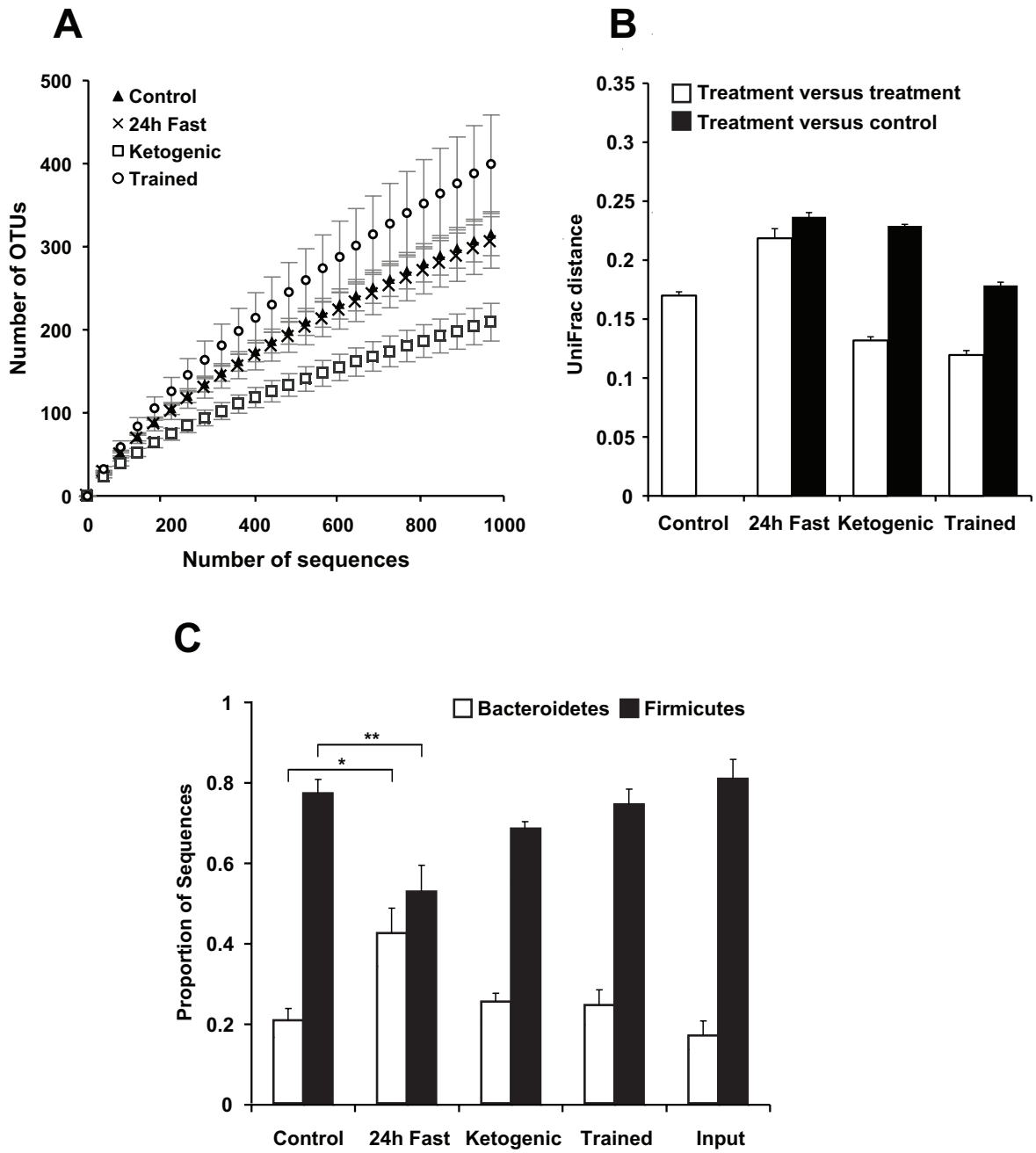

Fig. S2. 16S rRNA-based analysis of the effects of fasting, a ketogenic diet, or exercise on the cecal microbiota of CONV-D mice. (*A*) Rarefaction curves used to estimate bacterial diversity in the cecal microbiotas of CARB-fed control, 24-h fasted, ketogenic diet-fed and CARB-fed trained individuals (mean ± 95% confidence interval shown). The number of species-level phylotypes identified are plotted on the *y* axis (''species'' defined as organisms sharing ≥97% sequence identity in their 16S rRNA genes). (*B*) Average pairwise weighted UniFrac distance (a phylogeny-based measure of differences in community composition) for comparisons of individuals within a treatment (white bars) and comparisons of individuals between treatment versus CARB-fed untrained controls (black bars) [1,000 sequences per individual; Student's *t* test with Monte Carlo: 24-h fast (ns), ketogenic diet ($P < 0.001$), training ($P < 0.01$)]. (*C*) Proportional abundance of the Bacteroidetes and Firmicutes in the cecal microbiota of mice belonging to different treatment groups (mean ± SEM). ''Input'' refers to the cecal communities from conventionally raised donors that were transplanted to recipient germ-free mice. ''Control'' denotes conventionalized (CONV-D) recipients of the microbiota transplant who were consuming a standard polysaccharide-rich chow diet, and who were not subjected to exercise training in the gnotatorium. *, $P = 0.01$; **, $P = 0.007$ by 2-tailed Student's *t* test with unequal variance.

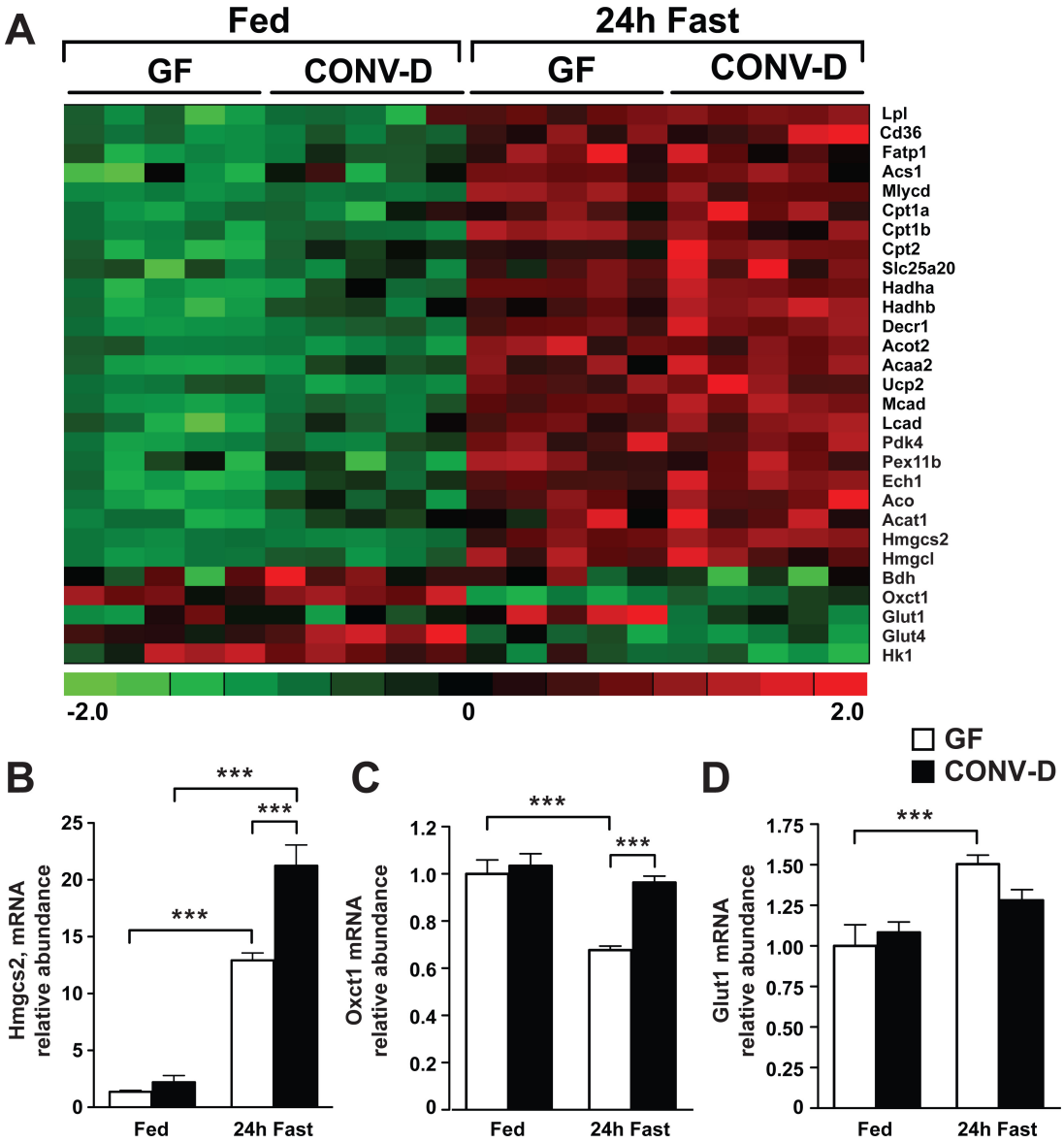

Fig. S3. Transcriptional response of the myocardium to a 24-h fast in GF versus CONV-D animals. (*A*) GeneChip analysis of genes that encode mediators of fatty acid oxidation, ketone body metabolism, and glucose uptake in CARB-fed and fasted GF and CONV-D mice. Red, up-regulated; green, down-regulated. Color key at the bottom of the heatmap indicates the standard deviation from the mean value across all samples. (*B–D*) qRT-PCR assays of selected transcripts in the hearts of GF and CONV-D CARB-fed and fasted animals. Values are expressed relative to GF CARB-fed controls. **, $P < 0.01$; ***, $P < 0.001$ (2-way ANOVA); $n =$ 5 animals per condition.

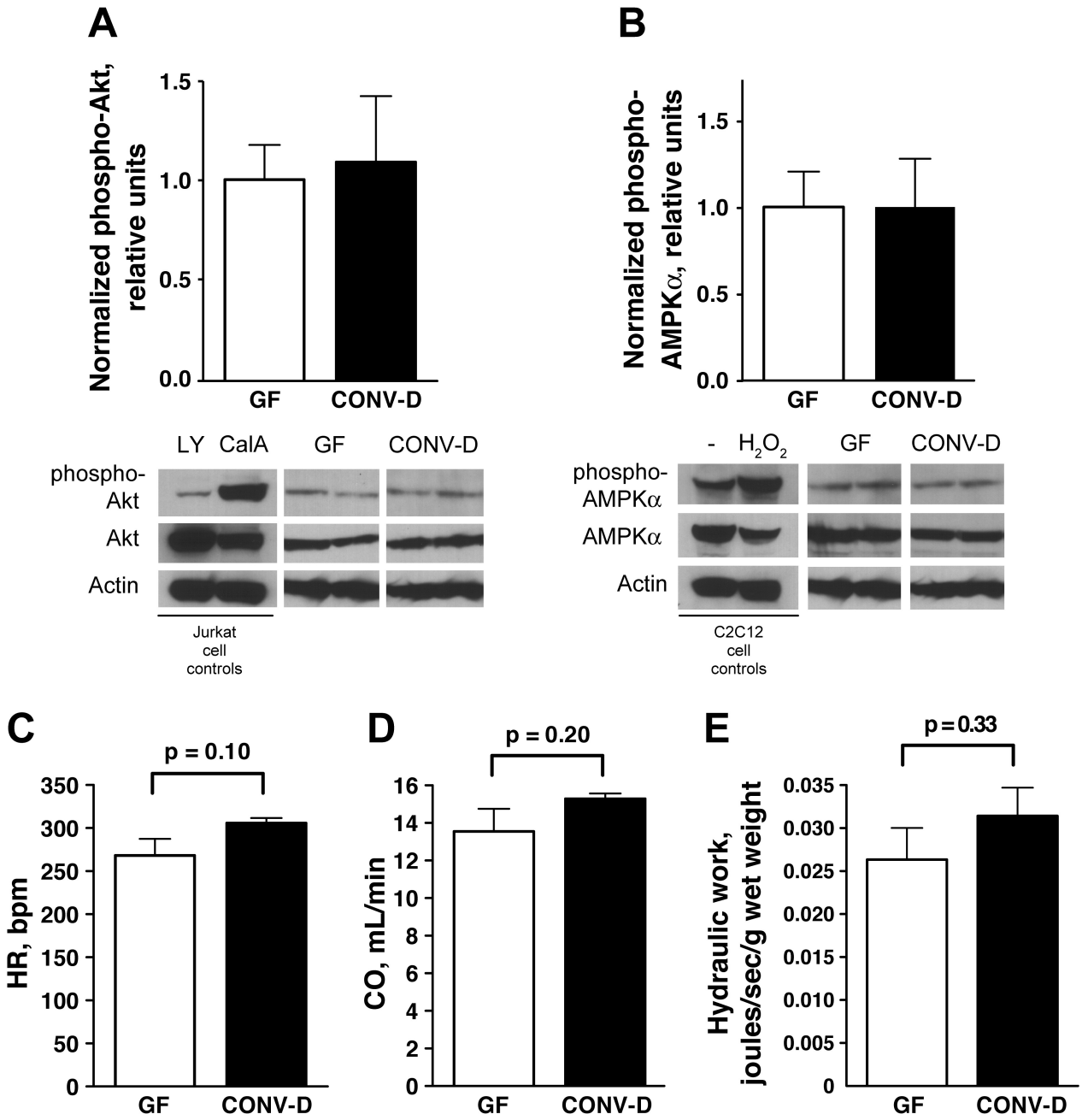

Fig. S4. Physiologic and biochemical analyses of hearts from fasted GF and CONV-D mice. (*A* and *B*) Studies of intact hearts. *A* shows the results of a Western blot analysis of the ratio of phospho-Akt1 (Ser-473) to Akt1 in the myocardium of fasted mice: No significant differences occur between fasted GF and CONV-D animals. Representative results from 2 mice are shown. Bar graphs plot mean values ± SEM, as defined by gel densitometry ($n = 10$ animals per group). Reference Akt controls consist of Jurkat cells stimulated with the PI3 kinase inhibitor LY294002 (abbreviated LY), or serum-starved Jurkat cells treated with the phosphatase inhibitor Calyculin A (abbreviated CalA). *B* presents an analysis of the Phospho-AMPKα (Thr-172) to AMPK ratio ($n = 10$ animals per group; the same as in *A*). Positive controls consist of untreated C2C12 mouse myoblast cells (low phospho-AMPKα) and cells treated for 5 min with 10 mM H_2O_2 (high phospho-AMPKα control). Note that for the GF and CONV-D fasting heart lysates, a separate and identically loaded SDS/PAGE gel was prepared to perform a single control actin Western blot. Because the Akt and AMPKα signals presented in *A* and *B* were obtained from the same GF and CONV-D fasting myocardial lysates, the normalizing actin bands obtained from these 4 lysates are presented under both Akt (*A*) and AMPKα (*B*). (*C–E*) Studies of isolated working hearts. The results of measurements of heart rate (HR; *C*), cardiac output (CO; *D*), and cardiac hydraulic work (*E*) plotted (mean values ± SEM; $n = 9$ animals per condition). There were no statistically significant differences between any of the treatment groups (Student's *t* test).

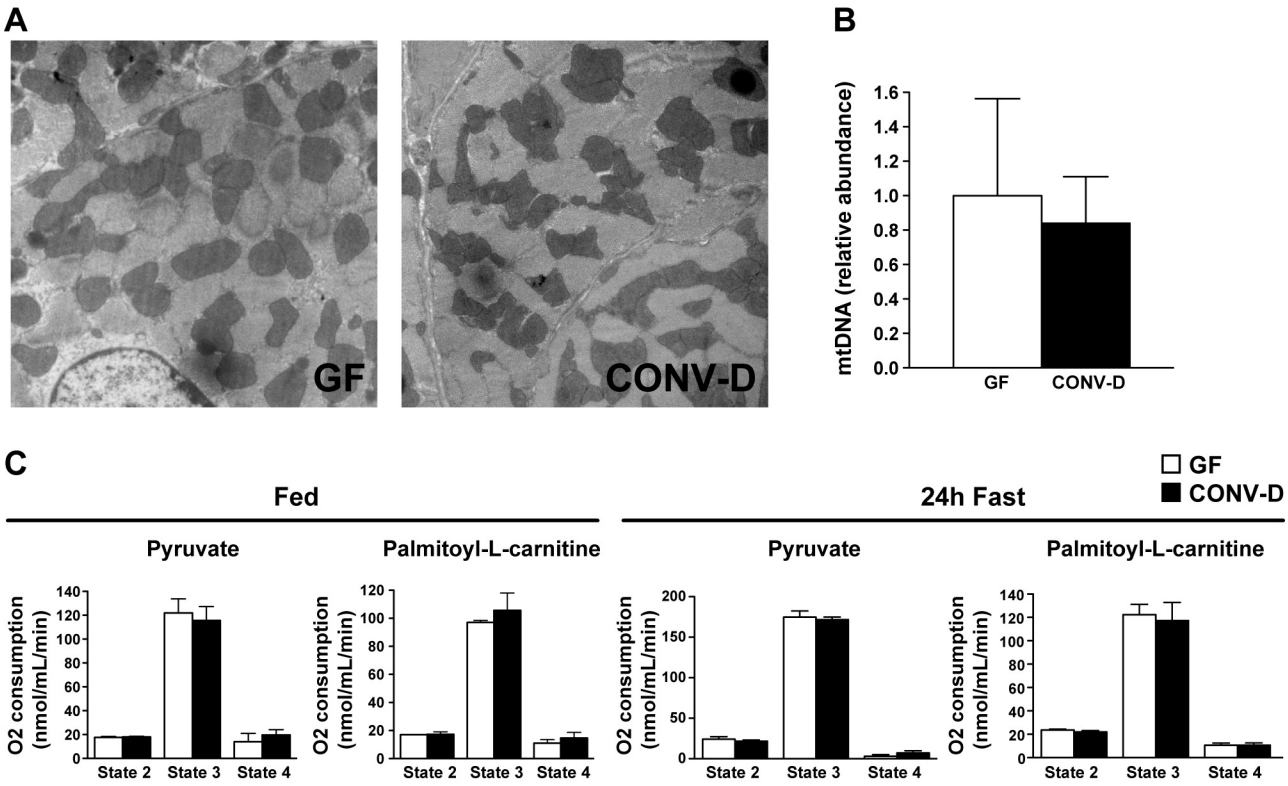

Fig. S5. Myocardial mitochondrial morphology, number, and function in GF and CONV-D mice. (*A*) Transmission EM micrographs of ventricles from CARB-fed GF and CONV-D mice showing similar mitochondrial morphology. (*B*) qPCR assays of the abundance of mitochondria in ventricles; abundance is defined as the ratio between mitochondrial and nuclear DNA using the *mtCytb* and *Rpl32* genes as PCR targets, respectively. (*C*) Measurements of oxygen consumption by isolated myocardial mitochondria using pyruvate and palmitoyl-L-carnitine as substrates under unstimulated (state 2), ADP-stimulated (state 3), and oligomycin-inhibited (state 4) conditions. There are no statistically significant differences between mitochondria isolated from the hearts of GF and CONV-D mice (2-way ANOVA). $n = 5$ animals per group for *B* and *C*.

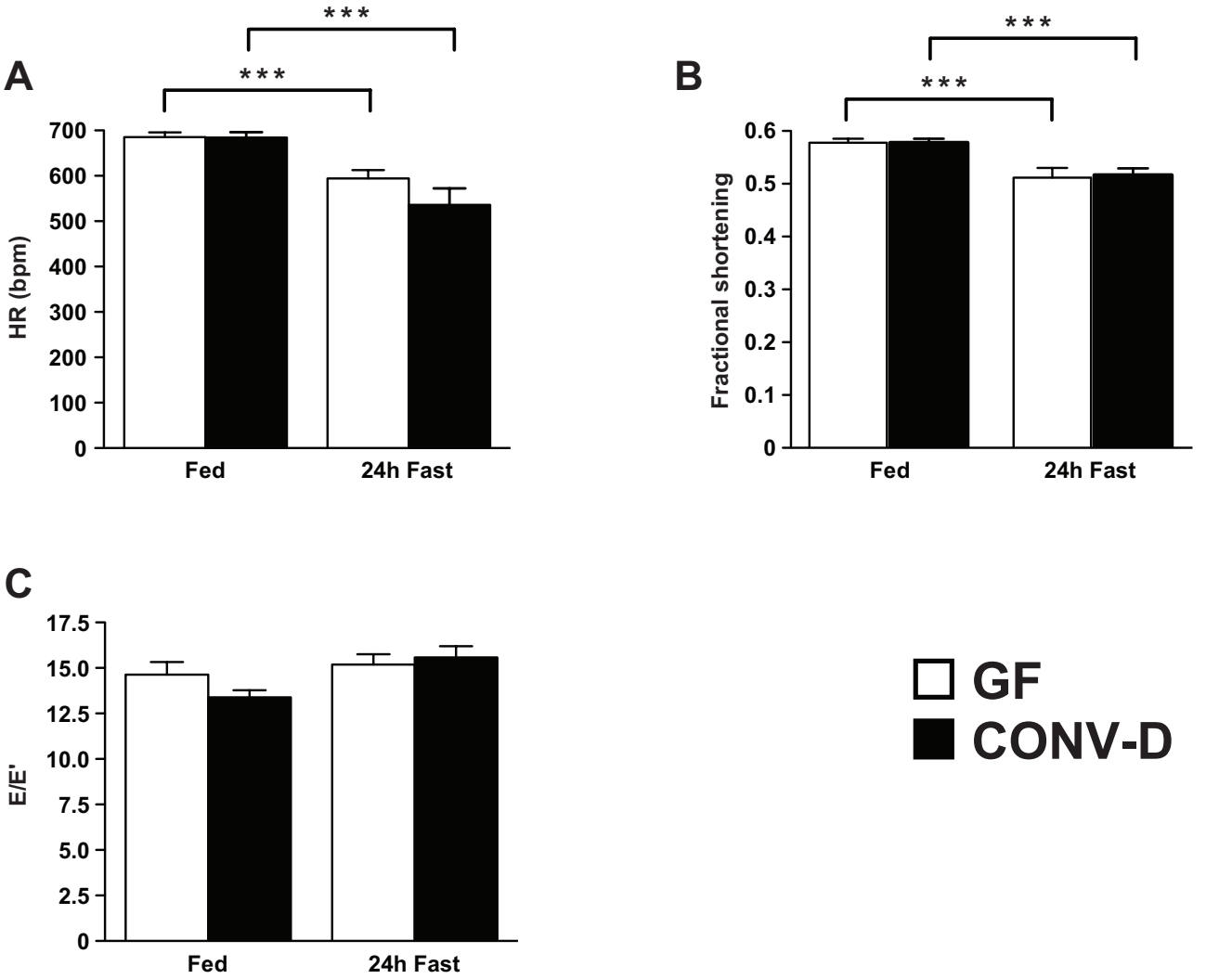

Fig. S6. Echocardiographic assessment of hearts from CARB-fed and fasted GF and CONV-D mice. In vivo echocardiographic determination of heart rate (*A*), fractional shortening (surrogate of systolic performance) (*B*), and E/E′ assessment of diastolic function (*C*). **, $P < 0.01$; ***, $P < 0.001$ (2-way ANOVA); $n = 5$ animals per condition.

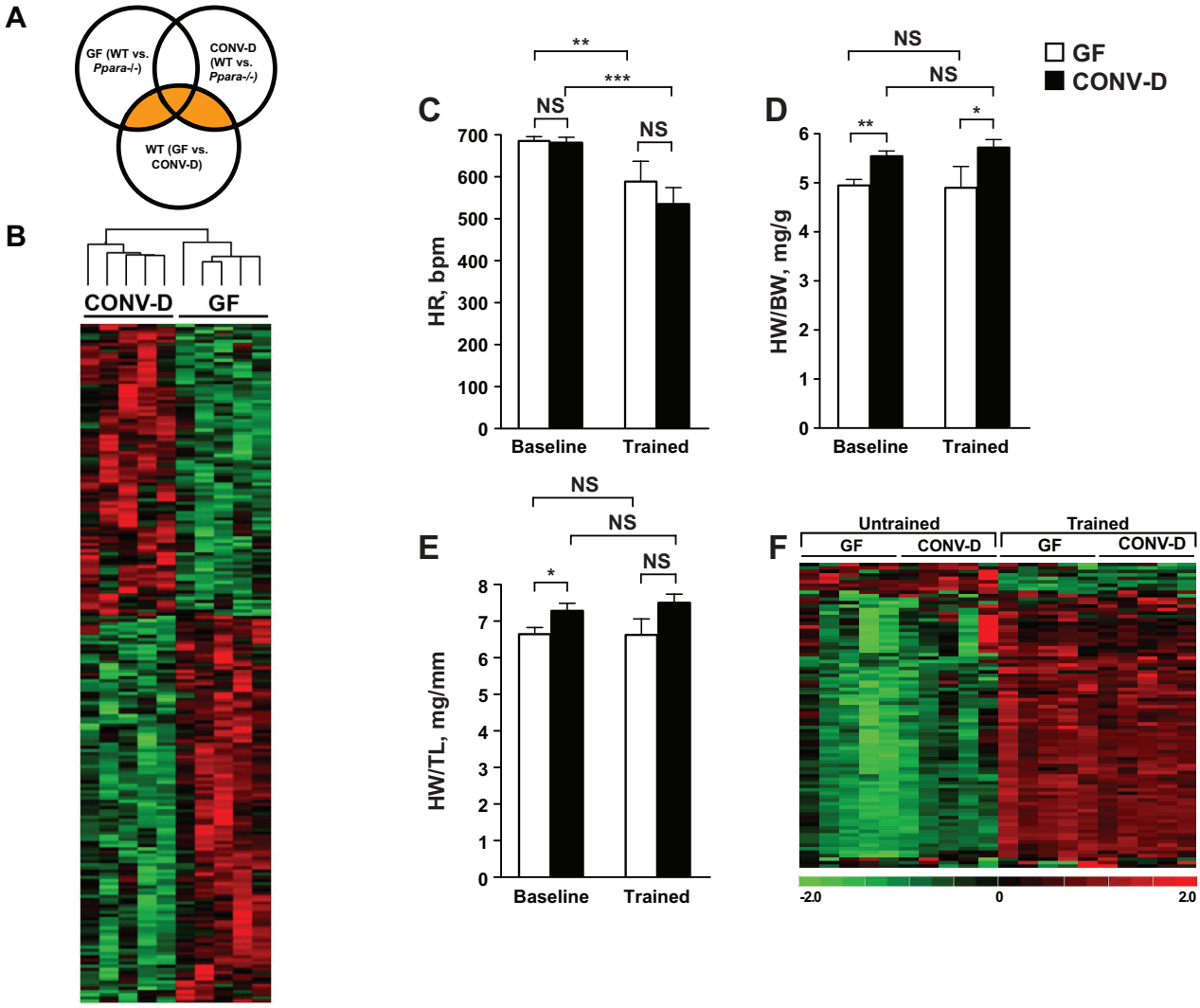

Fig. S7. Physiological and functional genomics analyses of the myocardial transcriptomes of CARB-fed untrained and trained GF and CONV-D mice. (*A*) A Venn diagram of the comparisons for untrained mice (see *SI Text* for additional details). (*B*) Heatmap, generated in dChip, of 170 microbiota-responsive myocardial genes in untrained mice (culled from the areas of the Venn diagram that are amber-colored in *A*). $n = 5$ animals per group. See Table S5 for a list of these genes. (*C–E*) Effects of endurance training in CARB-fed GF and CONV-D mice. (*C*) Echocardiographic assessment of heart rate (HR) in untrained and trained GF and CONV-D mice. (*D*) Heart weight (HW) to body weight (BW) ratio. (*E*) Heart weight to tibial length (TL) ratio. (*F*) GeneChip-derived Heatmap showing the relative levels of expression of nuclear-encoded mitochondrial genes involved in electron transport and oxidative phosphorylation. See Table S4 for a list of these genes.

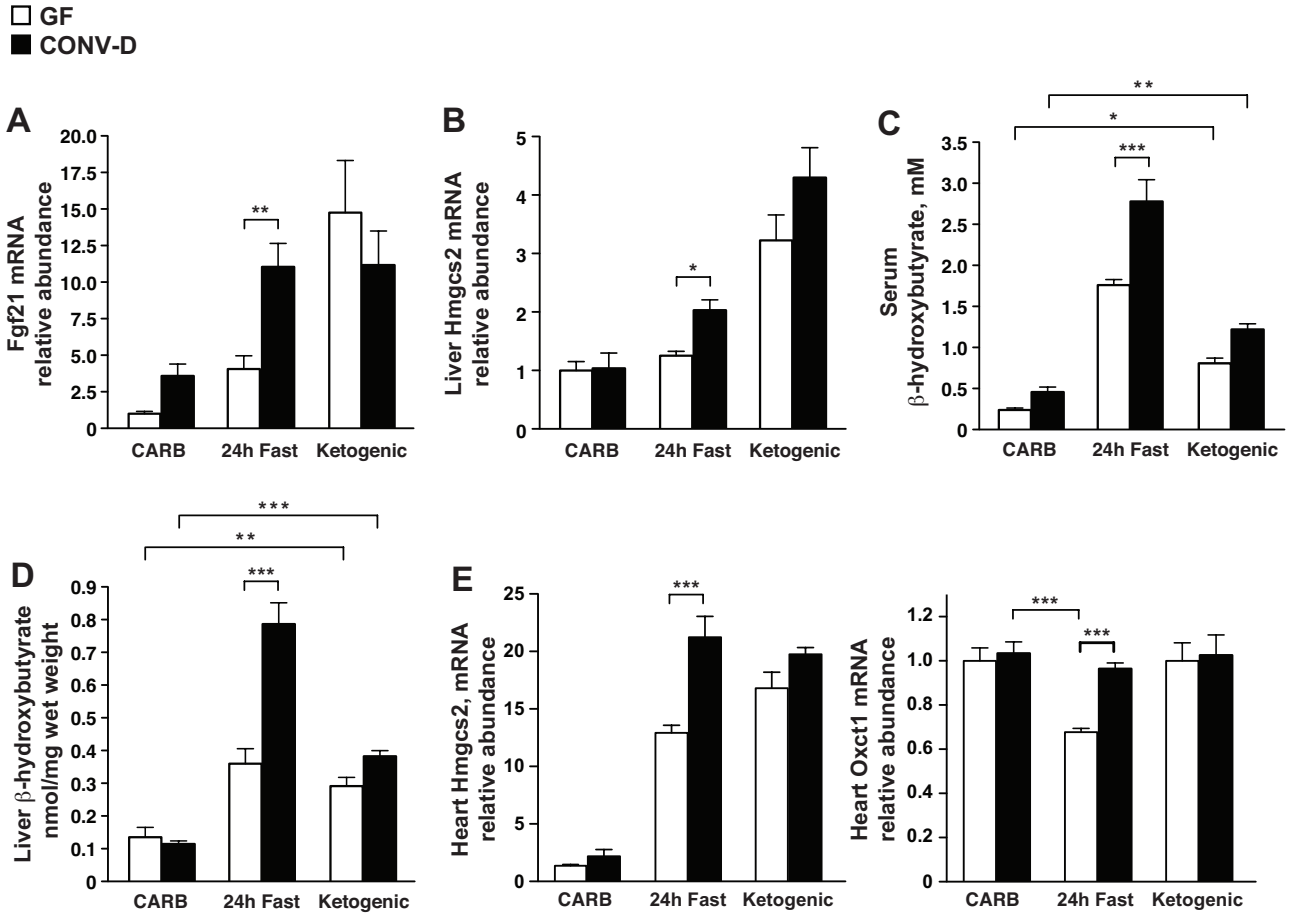

Fig. S8. Response of GF and CONV-D mice to a ketogenic diet. (*A* and *B*) qRT-PCR assays of *Fgf21* and *Hmgcs2* expression in the livers of GF and CONV-D animals fed a ketogenic diet for 30 days, compared with animals fed a standard CARB-diet, and those fasted for 24 h after being maintained on the CARB diet. Data are expressed relative to CARB-fed GF mice. *, $P < 0.05$; **, $P < 0.01$; NS, not significant (2-way ANOVA); $n = 5$ animals per condition. (*C* and *D*) Serum (*C*) and hepatic (*D*) levels of β-hydroxybutyrate ***, $P < 0.01$; $n = 6$ animals per condition. (*E*) Response within the myocardium of genes involved in ketone body metabolism to a ketogenic diet in GF and CONV-D mice: qRT-PCR assays of myocardial expression of *Hmgcs2* and *Oxct1*. ***, $P < 0.001$ (2-way ANOVA); $n = 5$ animals per condition.

Table S1. IPA analysis of pathways significantly enriched in GeneChip datasets of genes differentially expressed in wild-type hearts of GF or CONV-D mice (CARB-fed vs. 24-h fast)

Regulated pathways	*P* value (Fisher's exact test)	Regulated genes
GF		
ERK/MAPK signaling	0.001	PPARG, ETS1, MYCN, PPP1R14C, NRAS, PTK2B, SOS2, YWHAZ, PPP1CB, PPP1R3A, MKNK2, EIF4EBP1, PTK2, H3F3A, CREB1, DUSP4, YWHAQ (includes EG:22630), PPP2R5E, HSPB1
NRF2-mediated oxidative stress response	0.002	GSTA3, UBB, MAP2K7, NRAS, SOD1, PRDX1, HERPUD1, MAFK, DNAJA1, HMOX1, SOD2, GSTA4, GCLM, SQSTM1, AOX1, FKBP5, GSTM1 (includes EG:14862), GSTK1
IGF-1 signaling	0.003	PTK2, NRAS, CTGF, YWHAE, FOXO3, SOS2, CSNK2A1, IGF1R, YWHAZ, YWHAQ (includes EG:22630), RASA1
PTEN signaling	0.003	PTK2, NRAS, FOXO3, SOS2, CDKN1A, CSNK2A1, CHUK, LOC643751, CCND1, MAGI-3, PDGFRB
Hypoxia signaling in the cardiovascular system	0.005	VEGFA, UBB, NFKBIA, UBE2D2, CREB1, BIRC6, CSNK1D, UBE2D3, UBC
14–3-3-mediated signaling	0.007	NRAS, YWHAE, TUBB2A, YWHAZ, TUBA4A, VIM, PLCD1, PLCD3, PLCB4, TUBA1A, TUBA8, YWHAQ (includes EG:22630), PDGFRB
PI3K/AKT signaling	0.009	NRAS, NFKBIA, YWHAE, FOXO3, SOS2, CDKN1A, YWHAZ, YWHAQ (includes EG:22630), CHUK, PPP2R5E, CCND1, EIF4EBP1
Cell cycle: G2/M DNA damage checkpoint regulation	0.010	UBB, YWHAE, CDKN1A, TOP2A, YWHAZ, UBC
Integrin signaling	0.011	NRAS, SOS2, ITGA6, TSPAN2, PPP1CB, LOC643751, TTN, MYL7, ROCK1, PTK2, ARHGAP5, ACTR3, ARF4, RHOU, CAPN7, TSPAN4, ITGB5
Glycine, serine, and threonine metabolism	0.013	PLCD1, PLCD3, PLCB4, SHMT1, ALAS1, PDPR, GCAT, SARS
Calcium signaling	0.017	TPM1, CALR, HDAC2, TNNT2, TRDN, TPM4, MYH7, ATP2A2, MYL7, CAMK2D, CASQ1, CREB1, MYL4, ASPH, PPP3CA, CALM1
GM-CSF signaling	0.021	ETS1, CAMK2D, NRAS, CISH, SOS2, CCND1, PPP3CA
LPS/IL-1-mediated inhibition of RXR function	0.040	GSTA3, MAP2K7, FMO2, FMO5, HMGCS2, GSTA4, SULT1A1, NR5A2, ALAS1, ALDH18A1, SLC27A1, FABP5L2, FABP3, GSTM1 (includes EG:14862), GSTK1
Glutathione metabolism	0.040	GSTA3, GPX3, OPLAH, GSTA4, GCLM, GSTM1 (includes EG:14862), GSTK1
Wnt/β-catenin signaling	0.043	SOX4, UBB, GJA1, TCF4, CSNK1D, CCND1, CDH2, NLK, DKK3, CSNK2A1, PPP2R5E, UBC, WNT5A
B cell receptor signaling	0.043	ETS1, MAP2K7, CAMK2D, NRAS, NFKBIA, VAV3, SOS2, CREB1, CHUK, LOC643751, PPP3CA, CALM1
VEGF signaling	0.044	PTK2, ROCK1, VEGFA, NRAS, PTK2B, YWHAE, FOXO3, SOS2
CONV-D		
NRF2-mediated oxidative stress response	0.0003	UBB, MAP2K7, SOD1, PRDX1, CREBBP, MAFK, DNAJA1, GSTO1, HMOX1, SOD2, GSTA4, DNAJC14, GCLM, AOX1, FKBP5, GSTM1 (includes EG:14862)
Cell Cycle: G2/M DNA damage checkpoint regulation	0.002	UBB, YWHAE, CDKN1A, TOP2A, YWHAZ, UBC
Wnt/β-catenin signaling	0.003	SOX4, UBB, GJA1, TCF4, CREBBP, CSNK1D, CCND1, PPP2R1A, DKK3, CSNK2A1, PPP2R5E, UBC, WNT5A
PI3K/AKT signaling	0.006	PPP2R1A, NFKBIA, YWHAE, FOXO3, SOS2, CDKN1A, YWHAZ, PPP2R5E, CCND1, EIF4EBP1
Synthesis and degradation of ketone bodies	0.007	OXCT1, HMGCS2, HMGCS1
Glutathione metabolism	0.007	GPX3, OPLAH, GSTA4, GCLM, GSTM1 (includes EG:14862), GSTO1, IDH1
Hypoxia signaling in the cardiovascular system	0.008	VEGFA, UBB, NFKBIA, UBE2D2, CSNK1D, UBC, UBE2E1
PXR/RXR activation	0.009	SCD, CYP3A4, FOXO3, ALAS1, HMGCS2, GSTM1 (includes EG:14862), PPARGC1A
Hepatic fibrosis/hepatic stellate cell activation	0.010	VEGFA, CTGF, CYP2E1, IL10, IGF1R, MYL4, ECE1, MYH7, COL3A1, MYL7, PDGFRB
LPS/IL-1-mediated inhibition of RXR function	0.013	MAP2K7, FMO2, HMGCS2, FMO5, GSTO1, GSTA4, CYP3A4, SULT1A1, ALAS1, FABP4, SLC27A1, GSTM1 (includes EG:14862), HMGCS1
Actin cytoskeleton signaling	0.018	FGF16, F2R, SOS2, PFN2, RDX, PPP1CB, MYH7, LOC643751, TTN, MYL7, WASL (includes EG:8976), ACTR3, FGF12, MYL4
Xenobiotic metabolism signaling	0.020	MAP2K7, FMO2, CREBBP, FMO5, GSTO1, CYP1B1, HMOX1, PPP2R1A, CAMK2D, GSTA4, CYP3A4, SULT1A1, PPP2R5E, GSTM1 (includes EG:14862), PPARGC1A
Regulation of actin-based motility by rho	0.021	ACTR3, WASL (includes EG:8976), RHOU, PFN2, PPP1CB, MYL4, LOC643751, MYL7
Protein ubiquitination pathway	0.021	PSMB4, HSPA8, UBB, PSMC6, USP36, UBR2, UBE2D2, PSMC4, PSMD4, UBC, UBE2E1, HLA-C
IGF-1 signaling	0.026	CTGF, YWHAE, FOXO3, SOS2, CSNK2A1, IGF1R, YWHAZ

Regulated pathways	*P* value (Fisher's exact test)	Regulated genes
Ephrin receptor signaling	0.028	VEGFA, GNAI3, ACTR3, WASL (includes EG:8976), ITSN1, ABI1, SORBS1, SOS2, ADAM10, LOC643751, GNG5
p53 signaling	0.030	RB1, GADD45B, GADD45G, CDKN1A, CSNK1D, HIPK2, CCND1
PTEN signaling	0.030	FOXO3, SOS2, CDKN1A, CSNK2A1, LOC643751, CCND1, PDGFRB
Metabolism of xenobiotics by cytochrome P450	0.035	CYP3A4, GSTA4, CYP2E1, CYP4B1, ADH1C, MEST, GSTM1 (includes EG:14862), CYP1B1, GSTO1
Butanoate metabolism	0.044	LIPE, OXCT1, DCXR, HMGCS2, HMGCS1
Aryl hydrocarbon receptor signaling	0.044	RB1, NFIC, GSTA4, CDKN1A, NFIB, CCND1, GSTM1 (includes EG:14862), CYP1B1, GSTO

Table S2. IPA analysis of pathways significantly enriched in GeneChip datasets of genes differentially expressed in hearts of GF or CONV-D mice (wild-type vs. Pparα −/−)

Regulated pathways	*P* value (Fisher's Exact test)	Regulated genes
GF		
Fatty acid metabolism	0.0004	CPT2, ECH1, ACSL1
Butanoate metabolism	0.002	BDH1, ECH1
Propanoate metabolism	0.002	ECH1, ACSL1
Glycolysis/gluconeogenesis	0.006	ACSL1, FBP2
Synthesis and degradation of ketone bodies	0.014	BDH1
Fatty acid elongation in mitochondria	0.020	ECH1
LPS/IL-1-mediated inhibition of RXR function	0.022	CPT2, ACSL1
Pentose phosphate pathway	0.045	FBP2
CONV-D		
Fatty acid metabolism	2.51×10^{-6}	CPT2, ECH1, ACAA2, ACSL1, ALDH9A1
Butanoate metabolism	0.0001	BDH1, ECH1, ALDH9A1
Propanoate metabolism	0.0002	ECH1, ACSL1, ALDH9A1
Valine, leucine, and isoleucine degradation	0.0002	ECH1, ACAA2, ALDH9A1
LPS/IL-1-mediated inhibition of RXR function	0.0003	PPARA, CPT2, ACSL1, ALDH9A1
Fatty acid elongation in mitochondria	0.0004	ECH1, ACAA2
Glycolysis/gluconeogenesis	0.001	ACSL1, ALDH9A1, FBP2
Bile acid biosynthesis	0.002	ACAA2, ALDH9A1
β-alanine metabolism	0.004	ECH1, ALDH9A1
Lysine degradation	0.006	ECH1, ALDH9A1
Pyruvate metabolism	0.008	ACSL1, ALDH9A1
Synthesis and degradation of ketone bodies	0.021	BDH1
Tryptophan metabolism	0.023	ECH1, ALDH9A1
Ascorbate and aldarate metabolism	0.034	ALDH9A1
Circadian rhythm signaling	0.050	PER3

Table S3. IPA analysis of pathways significantly enriched in GeneChip datasets of genes differentially expressed in wild-type hearts of GF or CONV-D mice (untrained vs. trained)

Regulated pathways	*P* value (Fisher's Exact test)	Regulated genes
GF		
Hepatic fibrosis/hepatic stellate cell activation	9.77×10^{-8}	IGFBP4, MYH6, FN1, IL10, VEGFC, MMP2, IGFBP5, MYH7, MYL7, COL1A2, COL1A1, IGF1, CSF1, TGFB2, PDGFRA, ACTG2 (includes EG:72), TIMP2, PDGFRB, COL3A1, EGFR
Cell cycle: G2/M DNA damage checkpoint regulation	0.004	PCAF, YWHAE, YWHAB, TOP2A, YWHAZ, BRCA1
14–3-3-mediated signaling	0.005	TUBA8, YWHAE, YWHAB, PIK3R1, PDGFRA, YWHAZ, VIM, PDCD6IP, AXL, DDR1, EGFR, PDGFRB
IGF-1 signaling	0.007	IGFBP4, IGF1, YWHAE, YWHAB, PIK3R1, FOXO3, YWHAZ, PRKAG2, IGFBP5
Wnt/β -catenin signaling	0.011	SOX4, GJA1, SFRP2, FRZB, PPP2R1A, WIF1, CDH5, DKK3, TGFB2, FZD6, CD44, SFRP1, FZD2
ERK/MAPK signaling	0.023	ETS1, RAC2, MYCN, YWHAB, PIK3R1, CRKL, YWHAZ, PPP1CB, PPP1R3A, ELF4, PPP2R1A, PRKAG2, ELK3
Actin cytoskeleton signaling	0.028	RAC2, MYH6, FN1, F2R, ARPC5L (includes EG:81873), PIK3R1, CRKL, PPP1CB, LIMK2, MYH7, PDGFC, MYL7, ACTR3, ACTG2 (includes EG:72)
Complement system	0.041	C1R, CD55, C1QB, CFH
VEGF signaling	0.047	BCL2L1, YWHAE, PIK3R1, FOXO3, VEGFC, HIF1A, ACTG2 (includes EG:72)
CONV-D		
Hepatic fibrosis/hepatic stellate cell activation	0.001	COL1A2, COL1A1, CSF1, IL10, VEGFC, IGFBP5, MMP2, COL3A1, PDGFRB
Synthesis and degradation of ketone bodies	0.001	BDH1, ACAA1, OXCT1
Antigen presentation pathway	0.005	HLA-DQA1, HLA-DRB1, CD74, HLA-C
Cardiac β -adrenergic signaling	0.008	PPP2R1A, AKAP2, PDE7A, ADRBK2, PRKAG2, PPP1CB, ADCY7
Leukocyte extravasation signaling	0.010	ARHGAP5, GNAI3, TIMP3, TIMP4, CLDN5, PIK3R1, CYBB, MMP2, CTNND1
ERK/MAPK signaling	0.021	ETS1, PPP2R1A, PIK3R1, YWHAZ, PRKAG2, PPP1CB, ETS2, ELK3
IGF-1 signaling	0.025	PIK3R1, FOXO3, YWHAZ, PRKAG2, IGFBP5
Cell cycle: G2/M DNA damage checkpoint regulation	0.039	WEE1, TOP2A, YWHAZ
PXR/RXR activation	0.044	CYP3A4, FOXO3, PRKAG2, CES1 (includes EG:1066)
Bile acid biosynthesis	0.045	CYP3A4, ACAA1, ADH1C

Table S4. Genes included in the HeatMap shown in Fig. S7*F*

		GF		CONV-D		CARB-fed untrained		CARB-fed trained	
Gene	Accession no.	Fold change in CARB-fed trained vs. untrained	*P* value (*t* test)	Fold change in CARB-fed trained vs. untrained	*P* value (*t* test)	Fold change in CARB-fed untrained CONV-D vs. GF	*P* value (*t* test)	Fold change in CARB-fed trained CONV-D vs. GF	*P* value (*t* test)
NADH dehydrogenase (ubiquinone) 1 alpha subcomplex 10	NM_024197	1.52	<0.001	1.55	<0.001	1.03	0.727	1.05	0.360
NADH dehydrogenase (ubiquinone) 1 alpha subcomplex 11	AA596846	1.45	0.002	1.35	0.002	1.11	0.202	1.04	0.552
NADH dehydrogenase (ubiquinone) 1 alpha subcomplex, 1	NM_019443	1.19	0.042	1.13	0.118	1.03	0.756	−1.02	0.398
NADH dehydrogenase (ubiquinone) 1 alpha subcomplex, 12	NM_025551	1.43	0.013	1.38	<0.001	1.06	0.615	1.02	0.511
NADH dehydrogenase (ubiquinone) 1 alpha subcomplex, 13	AI429575	1.6	<0.001	1.3	<0.001	1.09	0.330	−1.13	0.015
NADH dehydrogenase (ubiquinone) 1 alpha subcomplex, 2	NM_010885	1.35	0.001	1.12	0.062	1.16	0.074	−1.04	0.161
NADH dehydrogenase (ubiquinone) 1 alpha subcomplex, 3	AV048277	1.45	0.001	1.24	0.005	1.15	0.085	−1.01	0.546
NADH dehydrogenase (ubiquinone) 1 alpha subcomplex, 4	BC011114	1.59	<0.001	1.59	<0.001	−1.03	0.686	−1.03	0.143
NADH dehydrogenase (ubiquinone) 1 alpha subcomplex, 5	NM_026614	2.4	<0.001	1.94	<0.001	1.12	0.214	−1.11	0.066
NADH dehydrogenase (ubiquinone) 1 alpha subcomplex, 6 (B14)	NM_025987	1.99	<0.001	1.76	<0.001	1.01	0.925	−1.12	0.038
NADH dehydrogenase (ubiquinone) 1 alpha subcomplex, 7 (B14.5a)	NM_023202	1.54	<0.001	1.45	0.002	1.07	0.432	1.01	0.714
NADH dehydrogenase (ubiquinone) 1 alpha subcomplex, 8	BC012416	1.78	<0.001	1.47	<0.001	1.2	0.042	−1.01	0.805
NADH dehydrogenase (ubiquinone) 1 alpha subcomplex, 9	NM_025358	1.2	0.015	1.13	0.048	1.07	0.359	1	0.934
NADH dehydrogenase (ubiquinone) 1 alpha subcomplex, assembly factor 1	BC018422	1.09	0.192	1.13	0.036	−1.01	0.884	1.03	0.551
NADH dehydrogenase (ubiquinone) 1 beta subcomplex 3	NM_025597	1.45	<0.001	1.44	<0.001	1.04	0.529	1.03	0.462
NADH dehydrogenase (ubiquinone) 1 beta subcomplex 4	BG968046	1.59	<0.001	1.38	<0.001	1.14	0.074	−1.02	0.361
NADH dehydrogenase (ubiquinone) 1 beta subcomplex 8	NM_026061	1.48	0.004	1.31	0.009	1.09	0.473	−1.04	0.167
NADH dehydrogenase (ubiquinone) 1 beta subcomplex, 10	BI905689	1.3	0.003	1.15	0.010	1.12	0.109	−1.01	0.777
NADH dehydrogenase (ubiquinone) 1 beta subcomplex, 11	BC027265	1.37	0.007	1.16	0.027	1.09	0.369	−1.08	0.007
NADH dehydrogenase (ubiquinone) 1 beta subcomplex, 2	NM_026612	1.76	<0.001	1.67	<0.001	1.01	0.899	−1.04	0.155
NADH dehydrogenase (ubiquinone) 1 beta subcomplex, 5	BC025155	1.19	0.010	1.12	0.013	1.07	0.199	1.02	0.567
NADH dehydrogenase (ubiquinone) 1 beta subcomplex, 7	NM_025843	1.85	0.001	1.7	<0.001	1.02	0.857	−1.07	0.125
NADH dehydrogenase (ubiquinone) 1 beta subcomplex, 9	AV161987	1.57	<0.001	1.4	<0.001	1.09	0.337	−1.03	0.280
NADH dehydrogenase (ubiquinone) 1, alpha/beta subcomplex, 1	AK010307	1.56	<0.001	1.43	<0.001	1.07	0.277	−1.01	0.572
NADH dehydrogenase (ubiquinone) 1, subcomplex unknown, 1	NM_025523	1.5	0.001	1.41	<0.001	1.05	0.542	−1.02	0.432
NADH dehydrogenase (ubiquinone) 1, subcomplex unknown, 2	NM_024220	1.08	0.218	1.11	0.095	1.06	0.364	1.09	0.128
NADH dehydrogenase (ubiquinone) Fe-S protein 1	BC006660	1.58	<0.001	1.4	<0.001	1.05	0.229	−1.07	0.001
NADH dehydrogenase (ubiquinone) Fe-S protein 2	BC016097	1.56	<0.001	1.34	<0.001	1.07	0.235	−1.08	0.015
NADH dehydrogenase (ubiquinone) Fe-S protein 3	BC027270	1.4	0.001	1.2	0.003	1.11	0.125	−1.05	0.054
NADH dehydrogenase (ubiquinone) Fe-S protein 4	NM_010887	1.5	<0.001	1.38	0.001	1.07	0.298	−1.01	0.831
NADH dehydrogenase (ubiquinone) Fe-S protein 5	NM_134104	1.41	0.001	1.31	<0.001	1.1	0.166	1.02	0.620
NADH dehydrogenase (ubiquinone) Fe-S protein 6	C88200	1.7	<0.001	1.35	<0.001	1.18	0.038	−1.06	0.124

Gene	Accession no.	GF		CONV-D		CARB-fed untrained		CARB-fed trained	
		Fold change in CARB-fed trained vs. untrained	*P* value (*t* test)	Fold change in CARB-fed trained vs. untrained	*P* value (*t* test)	Fold change in CARB-fed untrained CONV-D vs. GF	*P* value (*t* test)	Fold change in CARB-fed trained CONV-D vs. GF	*P* value (*t* test)
NADH dehydrogenase (ubiquinone) Fe-S protein 7	BC013503	2.16	<0.001	1.89	<0.001	1.11	0.227	−1.03	0.561
NADH dehydrogenase (ubiquinone) Fe-S protein 8	BC021616	1.39	0.001	1.29	0.011	1.1	0.309	1.03	0.557
NADH dehydrogenase (ubiquinone) flavoprotein 1	NM_133666	1.72	<0.001	1.53	0.001	1.05	0.639	−1.07	0.085
NADH dehydrogenase (ubiquinone) flavoprotein 2	BI692577	1.54	<0.001	1.32	0.001	1.12	0.162	−1.04	0.130
succinate dehydrogenase complex, subunit A, flavoprotein (Fp)	BF585357	1.11	0.037	1.06	0.106	1.05	0.242	1.01	0.638
succinate dehydrogenase complex, subunit B, iron sulfur (Ip)	BC013509	1.34	0.002	1.21	0.011	1.1	0.216	−1	0.840
succinate dehydrogenase complex, subunit C, integral membrane protein	AW107712	1.01	0.940	1.13	0.177	−1.05	0.488	1.07	0.621
succinate dehydrogenase complex, subunit D, integral membrane protein	AK013962	1.32	<0.001	1.26	<0.001	1.07	0.158	1.03	0.460
cytochrome b, ascorbate dependent 3	BB218627	−1.09	0.543	−1.19	0.109	1.02	0.878	−1.08	0.593
cytochrome b-245, alpha polypeptide	AK018713	−1.16	0.153	−1.34	0.006	1	0.969	−1.15	0.151
cytochrome b-245, beta polypeptide	AV373944	−2.16	<0.001	−2.25	<0.001	−1.04	0.573	−1.09	0.358
cytochrome b-5	NM_025797	1.02	0.693	1.02	0.570	1.04	0.375	1.04	0.197
cytochrome b-561	BC006732	1.04	0.783	1.41	0.096	−1.16	0.203	1.17	0.435
cytochrome c oxidase subunit IV isoform 1	NM_009941	1.25	0.022	1.08	0.397	1.16	0.217	−1	0.907
cytochrome c oxidase subunit IV isoform 2	NM_053091	−1.43	0.046	−1.67	0.012	−1.01	0.922	−1.18	0.316
cytochrome c oxidase subunit VIIa polypeptide 2-like	NM_009187	1.37	<0.001	1.21	0.006	1.01	0.762	−1.12	0.024
cytochrome c oxidase, subunit Va	NM_007747	1.14	0.056	−1.02	0.833	1.12	0.228	−1.04	0.421
cytochrome c oxidase, subunit Vb	NM_009942	1.31	0.013	1.21	0.017	1.05	0.625	−1.03	0.119
cytochrome c oxidase, subunit VI a, polypeptide 1	NM_007748	1.35	0.009	1.47	0.006	−1.21	0.163	−1.11	0.161
cytochrome c oxidase, subunit VI a, polypeptide 2	NM_009943	1.23	0.027	1.07	0.492	1.13	0.324	−1.02	0.396
cytochrome c oxidase, subunit VIb polypeptide 1	NM_025628	1.23	0.007	1.08	0.157	1.05	0.528	−1.09	0.038
cytochrome c oxidase, subunit VIc	NM_053071	1.25	0.028	1.07	0.555	1.16	0.302	−1.01	0.797
cytochrome c oxidase, subunit VIIa 1	AF037370	1.51	0.001	1.27	0.006	1.23	0.067	1.04	0.339
cytochrome c oxidase, subunit VIIa 2	NM_009945	1.27	0.005	1.12	0.173	1.09	0.382	−1.04	0.277
cytochrome c oxidase, subunit VIIc	NM_007749	1.14	0.133	1.04	0.520	1.08	0.456	−1.02	0.455
cytochrome c oxidase, subunit VIIIa	NM_007750	1.54	<0.001	1.62	<0.001	−1.09	0.291	−1.04	0.205
cytochrome c oxidase, subunit VIIIb	NM_007751	1.56	0.002	1.31	0.006	1.16	0.186	−1.02	0.372
cytochrome c oxidase, subunit VIIIc	AA144594	−2.05	<0.001	−1.73	<0.001	1.11	0.117	1.31	0.044
cytochrome c, somatic	NM_007808	1.39	0.001	1.4	<0.001	1.04	0.625	1.05	0.066
cytochrome c-1	NM_025567	1.16	0.023	1.03	0.747	1.1	0.339	−1.04	0.294
NADPH cytochrome B5 oxidoreductase	BC025438	1.03	0.553	1	0.997	1.01	0.896	−1.02	0.610
ubiquinol cytochrome c reductase core protein 2	BG075002	1.31	0.004	1.19	0.004	1.06	0.465	−1.04	0.212
ubiquinol-cytochrome c reductase (6.4kD) subunit	NM_025650	1.5	0.002	1.47	<0.001	−1	0.990	−1.02	0.339
ubiquinol-cytochrome c reductase binding protein	NM_026219	−1.28	0.001	−1.3	<0.001	1.08	0.068	1.07	0.123
ubiquinol-cytochrome c reductase core protein 1	AK004031	1.37	0.004	1.05	0.473	1.21	0.083	−1.08	0.162
ubiquinol-cytochrome c reductase hinge protein	AW106975	1.33	0.003	1.25	0.006	1.05	0.528	−1.01	0.541
ubiquinol-cytochrome c reductase, Rieske iron-sulfur polypeptide 1	AK003966	1.31	0.003	1.22	0.007	1.05	0.484	−1.02	0.400
ATP synthase mitochondrial F1 complex assembly factor 1	BB771055	1.79	<0.001	1.59	<0.001	1.18	0.001	1.05	0.242
ATP synthase mitochondrial F1 complex assembly factor 2	AI851949	1.67	<0.001	1.79	0.003	1.11	0.375	1.19	0.126

Gene	Accession no.	GF		CONV-D		CARB-fed untrained		CARB-fed trained	
		Fold change in CARB-fed trained vs. untrained	*P* value (*t* test)	Fold change in CARB-fed trained vs. untrained	*P* value (*t* test)	Fold change in CARB-fed untrained CONV-D vs. GF	*P* value (*t* test)	Fold change in CARB-fed trained CONV-D vs. GF	*P* value (*t* test)
ATP synthase, H + transporting mitochondrial F1 complex, beta subunit	NM_016774	−1.09	0.301	−1.25	0.137	1.14	0.335	−1	0.932
ATP synthase, H + transporting, mitochondrial F0 complex, subunit b, isoform 1	AK019459	1.41	<0.001	1.34	<0.001	1.06	0.323	1.01	0.795
ATP synthase, H + transporting, mitochondrial F0 complex, subunit c (subunit 9), isoform 1	NM_007506	1.41	0.002	1.29	0.002	1.1	0.264	−1	0.982
ATP synthase, H + transporting, mitochondrial F0 complex, subunit c (subunit 9), isoform 2	NM_026468	1.6	<0.001	1.46	<0.001	1.08	0.222	−1.01	0.313
ATP synthase, H + transporting, mitochondrial F0 complex, subunit c (subunit 9), isoform 3	AU080319	1.14	0.123	1.01	0.967	1.14	0.384	1.01	0.770
ATP synthase, H + transporting, mitochondrial F0 complex, subunit d	AF354051	1.21	0.021	1.04	0.680	1.13	0.287	−1.03	0.117
ATP synthase, H + transporting, mitochondrial F0 complex, subunit d	AV154755	−1.05	0.472	−1.13	0.275	1.14	0.274	1.06	0.173
ATP synthase, H + transporting, mitochondrial F0 complex, subunit F	NM_016755	1.37	0.001	1.2	0.011	1.08	0.339	−1.06	0.047
ATP synthase, H + transporting, mitochondrial F0 complex, subunit f, isoform 2	NM_020582	1.58	<0.001	1.49	<0.001	1.08	0.374	1.02	0.604
ATP synthase, H + transporting, mitochondrial F0 complex, subunit f, isoform 2	BG794445	1.08	0.181	1.03	0.676	1.08	0.338	1.03	0.248
ATP synthase, H + transporting, mitochondrial F0 complex, subunit g	NM_013795	1.31	0.010	1.29	0.003	1.03	0.678	1.02	0.765
ATP synthase, H + transporting, mitochondrial F0 complex, subunit s	NM_026536	1.49	<0.001	1.51	0.009	−1.01	0.913	−1	0.982
ATP synthase, H + transporting, mitochondrial F1 complex, alpha subunit, isoform 1	C78762	1.43	0.023	−1.01	0.956	1.17	0.412	−1.23	0.098
ATP synthase, H + transporting, mitochondrial F1 complex, delta subunit	BC008273	1.48	<0.001	1.27	0.001	1.07	0.251	−1.1	0.033
ATP synthase, H + transporting, mitochondrial F1 complex, epsilon subunit	NM_025983	1.8	<0.001	1.83	<0.001	−1.04	0.744	−1.02	0.426
ATP synthase, H + transporting, mitochondrial F1 complex, gamma polypeptide 1	NM_020615	1.43	0.001	1.26	0.012	1.14	0.173	1	0.897
ATP synthase, H + transporting, mitochondrial F1 complex, O subunit	NM_138597	1.34	0.007	1.21	0.024	1.08	0.402	−1.02	0.170
ATP synthase, H + transporting, mitochondrial F1 complex, O subunit /// similar to ATP synthase, H + transporting, mitochondrial F1 complex, O subunit	AV066932	−1.8	0.037	−1.65	0.009	−1.02	0.902	1.07	0.504
ATP synthase, H + transporting, mitochondrial F1F0 complex, subunit e	NM_007507	1.45	0.003	1.26	<0.001	1.12	0.222	−1.02	0.452

Table S5. Genes included in the HeatMap shown in Fig. S7*B*

Gene	Accession Number	Fold change in CARB-fed CONV-D vs. GF	*P* value (Student's *t* test)
Histocompatibility 2, class II antigen A, alpha	AV018723	2.84	0.02
Thioredoxin interacting protein	AF173681	2.31	0.05
Uncoupling protein 3 (mitochondrial, proton carrier)	AF053352	2.26	0.02
Ia-associated invariant chain	BC003476	2.04	0.01
D site albumin promoter binding protein	BC018323	1.83	0.01
Histocompatibility 2, class II antigen E beta	NM_010382	1.81	0.03
Tropomodulin 4	NM_016712	1.81	0.005
Prostaglandin D2 synthase (brain)	AB006361	1.71	0.03
Carboxypeptidase X 2 (M14 family)	AF017639	1.65	0.02
Pyruvate dehydrogenase kinase, isoenzyme 4	NM_013743	1.63	0.05
Angiopoietin-like 4	NM_020581	1.61	0.02
Glutamic pyruvate transaminase (alanine aminotransferase) 2	BI648645	1.59	0.02
Sterol carrier protein 2, liver	C76618	1.56	0.04
Sodium channel, type IV, beta	BE993937	1.56	0.0002
p21 (CDKN1A)-activated kinase 6	BB818370	1.55	0.001
Guanine nucleotide binding protein, beta 3	NM_013530	1.49	0.04
Zinc finger protein 306	BC007473	1.47	0.02
PRP19/PSO4 homolog (*Saccharomyces cerevisiae*)	BC004070	1.47	0.05
SH2 domain containing 4A	AK008803	1.45	0.004
InaD-like (*Drosophila*)	AV287690	1.42	0.004
RNA polymerase 1–2	NM_009086	1.4	0.01
F-box and leucine-rich repeat protein 17	AK018254	1.4	0.04
Nuclear receptor subfamily 1, group D, member 1	W13191	1.39	0.002
Myosin Vb	AW546331	1.37	0.002
Solute carrier family 16 (monocarboxylic acid transporters), member 10	BB735478	1.36	0.05
Stomatin	AF093620	1.35	0.05
SH3-domain binding protein 5 (BTK-associated)	BQ179335	1.35	0.03
Microtubule-associated protein tau	M18775	1.35	0.004
Ankyrin 3, epithelial /// RIKEN cDNA 2900054D09 gene	BB628935	1.35	0.001
FYVE and coiled-coil domain containing 1	BM123442	1.35	0.03
Coenzyme Q3 homolog, methyltransferase (yeast)	BB108855	1.33	0.0017
Protein kinase inhibitor, alpha	AK010212	1.32	0.01
Enoyl coenzyme A hydratase 1, peroxisomal	NM_016772	1.32	0.01
CD2 antigen (cytoplasmic tail) binding protein 2	NM_027353	1.31	0.04
Cell cycle progression 1	BC006717	1.31	0.05
RNA binding motif and ELMO domain 1	BC016193	1.31	0.03
Arylacetamide deacetylase-like 1	AV369935	1.31	0.01
Sorting nexin 5	NM_024225	1.3	0.0003
Ankyrin repeat domain 1 (cardiac muscle)	AK009959	1.29	0.005
Mitogen-activated protein kinase kinase kinase 4	AV079128	1.29	0.05
Fibroblast growth factor 16	NM_030614	1.28	0.03
Synaptojanin 2	BE944213	1.28	0.05
Ectonucleoside triphosphate diphosphohydrolase 5	BB309883	1.28	9.E-06
Fumarylacetoacetate hydrolase	NM_010176	1.27	0.02
Diacylglycerol *O*-acyltransferase 2	AK002443	1.27	0.01
Influenza virus NS1A binding protein	BC004092	1.26	0.005
Hydroxyacyl-coenzyme A dehydrogenase/3-ketoacyl-coenzyme A thiolase/enoyl-coenzyme A hydratase (trifunctional protein), beta subunit	BG866501	1.26	0.01
Ubiquitin-conjugating enzyme E2R 2	AV054417	1.25	0.01
Carnitine palmitoyltransferase 2	NM_009949	1.25	0.002
Peroxisomal biogenesis factor 11a	NM_011068	1.25	0.05
Malonyl-CoA decarboxylase	NM_019966	1.25	0.001
Cellular repressor of E1A-stimulated genes 1	BC027426	1.24	0.03
Myeloid ecotropic viral integration site-related gene 1	BB207647	1.24	0.01
2,4-dienoyl CoA reductase 1, mitochondrial	NM_026172	1.23	0.01
Lipin 1	AK014526	1.23	0.001
Acetyl-coenzyme A acyltransferase 2 (mitochondrial 3-oxoacyl-coenzyme A thiolase)	AK002555	1.23	0.02
Cytoplasmic FMR1 interacting protein 2	AK005148	1.23	0.02
Progestin and adipoQ receptor family member IX	AV103696	1.23	0.04
Ly6/neurotoxin 1	NM_011838	1.21	0.02

Gene	Accession Number	Fold change in CARB-fed CONV-D vs. GF	*P* value (Student's *t* test)
Very low density lipoprotein receptor	NM_013703	1.21	0.05
Epoxide hydrolase 2, cytoplasmic	NM_007940	1.21	0.05
Tumor necrosis factor receptor superfamily, member 19-like	BB396291	1.21	0.003
Tumor rejection antigen gp96	NM_011631	1.2	0.02
Arginine-rich, mutated in early stage tumors	AK014338	1.2	0.05
Sec61 alpha 1 subunit (*S. cerevisiae*)	BC003707	−1.21	0.04
Nudix (nucleoside diphosphate linked moiety X)-type motif 2	NM_025539	−1.21	0.05
Serine carboxypeptidase 1	AK014680	−1.21	0.05
Secreted frizzled-related sequence protein 1	AK008943	−1.21	0.05
Fibulin 2	BF228318	−1.23	0.05
Actin-related protein 2/3 complex, subunit 1B	BE979985	−1.24	0.04
Heart and neural crest derivatives expressed transcript 2	NM_010402	−1.24	0.005
Filamin, alpha	BM233746	−1.24	0.03
Actinin, alpha 1	BE853286	−1.24	0.05
Cofilin 1, non-muscle	AV148266	−1.24	0.03
Diaphorase 1 (NADH)	NM_029787	−1.25	0.01
Matrix-remodelling associated 8	BB765827	−1.25	0.02
CD34 antigen	NM_133654	−1.26	0.05
Lysyl oxidase-like 1	AF357006	−1.26	0.01
Laminin, alpha 4	BB053010	−1.27	0.03
SWI/SNF-related, matrix-associated, actin-dependent regulator of chromatin, subfamily d, member 2	NM_031878	−1.28	0.02
Ras homolog gene family, member C	NM_007484	−1.28	0.05
Notch gene homolog 2 (Drosophila)	AI787996	−1.28	0.01
Sprouty homolog 1 (*Drosophila*)	NM_011896	−1.29	0.02
Biglycan	BC019502	−1.29	0.01
Matrix metalloproteinase 2	BF147716	−1.29	0.03
Low density lipoprotein receptor-related protein 1	NM_008512	−1.29	0.03
Sulfatase 1	BB065799	−1.29	0.04
Casein kinase 1, delta	NM_139059	−1.3	0.002
Insulin-like growth factor binding protein 7	AI481026	−1.3	0.003
Uncoupling protein 2 (mitochondrial, proton carrier)	BC012697	−1.3	0.04
Coronin 7	AV025980	−1.3	0.04
Potassium voltage-gated channel, shaker-related subfamily, member 5	NM_008419	−1.31	0.003
Destrin	NM_019771	−1.32	0.01
Dermatopontin	NM_019759	−1.32	0.03
Transgelin 2	C76322	−1.32	0.01
Cysteine-rich protein 1 (intestinal)	NM_007763	−1.34	0.02
Programmed cell death 6 interacting protein	AJ005074	−1.34	0.03
G protein-coupled receptor kinase 5	BC019379	−1.34	0.0004
CD9 antigen	NM_007657	−1.35	0.03
Reticulocalbin 3, EF-hand calcium binding domain	BC025602	−1.35	0.01
Dihydropyrimidinase-like 3	AV162270	−1.35	0.0048
Immunoglobulin superfamily containing leucine-rich repeat	NM_012043	−1.36	0.02
Integral membrane protein 2A	BI966443	−1.36	0.01
Expressed sequence AA536743	BI248354	−1.36	0.01
Polycystic kidney disease 2	BB249222	−1.36	0.001
Tetraspan 2	BC007185	−1.37	0.03
procollagen C-proteinase enhancer protein	NM_008788	−1.37	0.001
Glutamine fructose-6-phosphate transaminase 2	NM_013529	−1.38	0.02
Annexin A2	NM_007585	−1.38	0.005
Procollagen C-proteinase enhancer protein	BB250811	−1.38	0.001
Secreted acidic cysteine-rich glycoprotein	NM_009242	−1.38	0.01
Protein tyrosine phosphatase, nonreceptor type substrate 1	AB018194	−1.39	0.05
Lumican	AK014312	−1.39	0.02
Sulfatase 2	AK008108	−1.39	0.003
Tissue inhibitor of metalloproteinase 2	M93954	−1.39	0.01
Filamin A-interacting protein 1	AV241894	−1.39	0.01
nidogen 1	X14480	−1.4	0.02
Procollagen, type VI, alpha 1	NM_009933	−1.4	0.0003
Angiotensin converting enzyme	M55333	−1.4	0.0004
Matrix metalloproteinase 2	NM_008610	−1.41	0.001
Calsequestrin 1	NM_009813	−1.41	0.03

Gene	Accession Number	Fold change in CARB-fed CONV-D vs. GF	*P* value (Student's *t* test)
Cell division cycle 20 homolog (*S. cerevisiae*)	NM_023223	−1.42	0.03
Transcribed locus	AA266723	−1.42	0.04
Vimentin	M24849	−1.42	0.01
Epimorphin	NM_007941	−1.43	0.01
Cysteine and glycine-rich protein 1	BF124540	−1.43	0.000
PDZ and LIM domain 5	NM_019808	−1.43	0.05
Dynein, cytoplasmic, light chain 1	NM_019682	−1.44	0.003
A disintegrin-like and metalloprotease (reprolysin type) with thrombospondin type 1 motif, 2	BM125019	−1.44	0.01
Procollagen, type XIV, alpha 1	AJ131395	−1.45	0.01
Syndecan 4	BC005679	−1.45	0.01
Thrombospondin 1	AI385532	−1.45	0.03
EF hand domain containing 1	BC019531	−1.47	0.003
Steroid 5 alpha-reductase 2-like	BB825787	−1.47	0.01
Cartilage intermediate layer protein, nucleotide pyrophosphohydrolase	BE630003	−1.5	0.05
Cytokine inducible SH2-containing protein	NM_009895	−1.51	0.04
Anthrax toxin receptor 1	AF378762	−1.51	0.01
LPS-induced TN factor	AV360881	−1.52	0.001
Coatomer protein complex, subunit gamma 2, antisense 2	BE653037	−1.52	0.03
Fibronectin type III domain containing 1	AK003938	−1.53	0.02
Follistatin-like 1	BI452727	−1.54	0.01
Latent transforming growth factor beta binding protein 3	NM_008520	−1.57	0.003
Microfibrillar associated protein 5	NM_015776	−1.58	0.0002
Procollagen, type XVIII, alpha 1	D17546	−1.58	0.03
Insulin-like growth factor 2	NM_010514	−1.58	0.002
Fatty acid binding protein 5, epidermal	BC002008	−1.59	0.004
Procollagen, type VI, alpha 2	BI455189	−1.59	0.001
CD248 antigen, endosialin	NM_054042	−1.6	0.001
Periostin, osteoblast specific factor	BI110565	−1.62	0.01
Latent transforming growth factor beta binding protein 2	NM_013589	−1.65	0.05
Fibrillin 1	NM_007993	−1.65	0.001
Cysteine and glycine-rich protein 2	NM_007792	−1.67	0.02
Ral guanine nucleotide dissociation stimulator,-like 1	NM_016846	−1.67	0.02
Procollagen, type I, alpha 1	U08020	−1.69	0.0018
Myosin, light polypeptide 9, regulatory	AK007972	−1.69	0.03
Fibronectin 1	BC004724	−1.71	0.004
Procollagen, type V, alpha 2	AV229424	−1.74	0.0002
Microfibrillar associated protein 5	NM_015776	−1.74	0.004
S100 calcium binding protein A4	D00208	−1.79	0.001
Stearoyl-coenzyme A desaturase 2	BG060909	−1.8	0.0001
Discoidin domain receptor family, member 1	BB234940	−1.82	0.03
Procollagen, type V, alpha 1	AW744319	−1.85	0.01
Matrix metalloproteinase 14 (membrane-inserted)	NM_008608	−1.94	0.003
Actin, alpha 2, smooth muscle, aorta	NM_007392	−1.99	0.001
Neurotensin	NM_024435	−1.99	0.0004
A disintegrin-like and metalloprotease (reprolysin type) with thrombospondin type 1 motif, 2	BG073461	−2.15	0.002
Procollagen, type III, alpha 1	AW550625	−2.16	0.004
Procollagen, type I, alpha 2	BF227507	−2.17	0.0002
Elastin	BB229377	−2.27	0.01
Microfibrillar-associated protein 4	BC022666	−3.62	0.003

Table S6. Primer sets used in this study

Gene	GenBank accession no.	Primer	Primer sequences	Amplicon size, bp
mtCytb	BC004586	Forward	5′-CCTTCATACCTCAAAGCAACGA	85
		Reverse	5′-GATAAGTAGGTTGGCTACTAGGATTCAGT	
Fgf21	NM_020013	Forward	5′-CCAGATGTGGGCTCCTCTGAC	101
		Reverse	5′-AGAAACAGCCCTAGATTCAGGAAGAGT	
Glut1	NM_011400	Forward	5′-TCGTTGGCATCCTTATTGC	91
		Reverse	5′-ACGAAGACGACACTGAGCAG	
Hmgcs2	NM_008256	Forward	5′-TGGTTCAAGACAGGGACACAGAAC	98
		Reverse	5′-AGAGGAATACCAGGGCCCAACAAT	
Rpl32	NM_172086	Forward	5′-CCTCTGGTGAAGCCCAAGATC	102
		Reverse	5′-TCTGGGTTTCCGCCAGTTT	
Oxct1	NM_024188	Forward	5′-TGGCCAACTGGATGATACCTGG	97
		Reverse	5′-TCCATGGTGACCACCACTTTGG	
Ppara	NM_011144	Forward	5′-ACTACGGAGTTCACGCATGTG	76
		Reverse	5′-TTGTCGTACACCAGCTTCAGC	
Pnpla2	NM_025802	Forward	5′-TACCAGCCAAGCTCCAAGTTGT	113
		Reverse	5′-GGTCCTATGTCCTCATTCCACAGCAT	